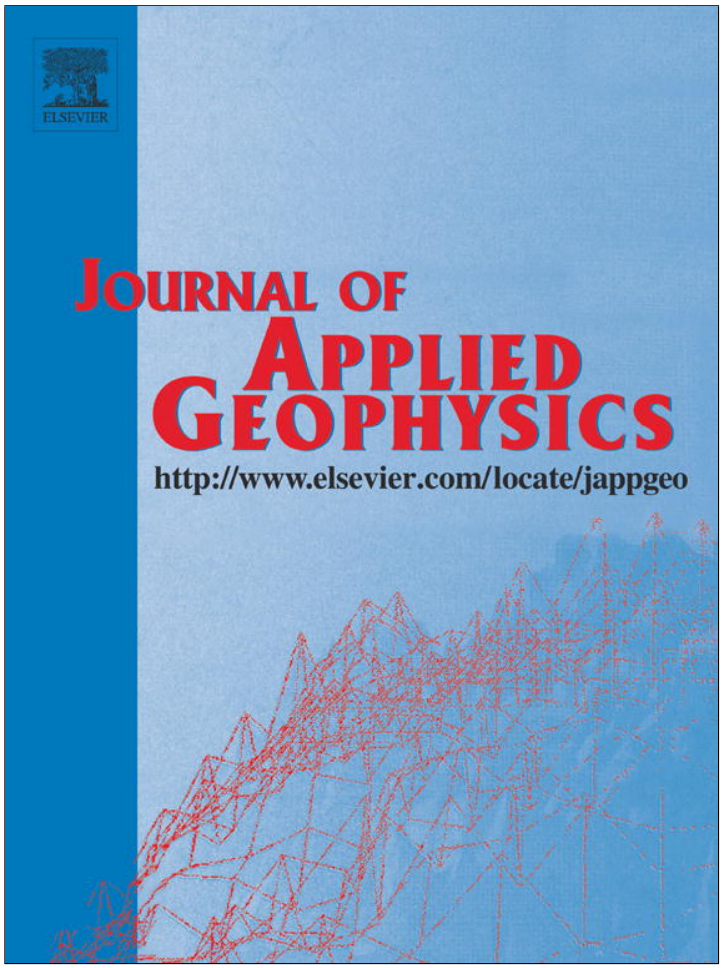

(This is a sample cover image for this issue. The actual cover is not yet available at this time.)

Journal of Applied Geophysics 83 (2012) 57–64

Contents lists available at SciVerse ScienceDirect

Journal of Applied Geophysics

journal homepage: www.elsevier.com/locate/jappgeo

Location and characterization of the Sancti Spiritus Fort from geophysical investigations

Néstor Bonomo [a], Ana Osella [a,*], Patricia Martinelli [a], Matías de la Vega [a], Gabriel Cocco [b], Fabian Letieri [c], Guillermo Frittegotto [d]

[a] Grupo de Geofísica Aplicada y Ambiental, Departamento de Física, Facultad de Ciencias Exactas y Naturales, Universidad de Buenos Aires/IFIBA-CONICET, Argentina
[b] Departamento de Estudios Etnográficos y Coloniales de Santa Fe, Argentina
[c] Departamento de Arqueología, Museo Histórico Provincial de Rosario, Argentina
[d] Universidad Abierta Interamericana, Argentina

ARTICLE INFO

Article history:
Received 13 October 2011
Accepted 28 April 2012
Available online 15 May 2012

Keywords:
Ground penetrating radar
Electromagnetic induction
Electrical imaging
Archaeological prospecting
Sancti Spiritus Fort
Argentina

ABSTRACT

A geophysical investigation was carried out to locate and characterize the remains of the Sancti Spiritus Fort, the first European settlement in the South Cone of America (1527–1529). In an initial stage, we used three complementary methods, ground penetrating radar, multifrequency electromagnetic induction and dipole–dipole electric profiling, to increase the possibility of detecting the structures of the Fort whose physical properties were expected to be similar to those of the surrounding soil, as they were constructed with raw earth probably extracted from it. From different views of the data, a number of electromagnetic signals apparently related to these structures were identified. Test excavations confirmed these hypotheses and showed that the structures were poorly preserved. Furthermore, they were almost indistinguishable through direct inspection of the excavated sections of soil, and very difficult to track. Therefore, in a second stage of geophysical studies, we acquired high-density grids of GPR data at relevant areas, looking for more detailed information about the structures. The results of these studies allowed to determine with precision their continuity through the site and also to interpret a number of areas which had remained unclear from the first survey. Extensive archaeological excavations were designed from the geophysical maps and carried out. From them, the geophysical interpretations were fully confirmed, and the presence of structural elements of previous and later native settlements was established.

1. Introduction

Geophysical methods are increasingly being used for the detection and characterization of archaeological structures. One advantage of methods such as Ground Penetrating Radar (GPR), small-loop multifrequency electromagnetic induction (EMI or SLEM) and geoelectrical profiling is that they allow prospecting large subsoil volumes in relatively short times, and often have a good detection capacity of the structures. Furthermore, these methods help to preserve the historical objects, because they minimally disturb the soil and provide detailed maps that can be used to plan excavations (Bongiovanni et al., 2008; Bonomo et al., 2010).

The Sancti Spiritus Fort was the first Spanish settlement in the South Cone of America. The establishment of this first enclave meant the beginning of a complex process that was decisive for the life of societies living in the region: the beginning of the Spanish conquest and colonial period (16th century), which was extensively treated through historical documentation. The Fort was founded by Sebastian Cabot in 1527 and had a brief existence, until 1529, when it was attacked and burned down by native population (Astiz, 1998; Astiz and Tomé, 1987; Carbia, 1914; Outes, 1902; Zapata Gollan, 1979). Though the general region where it was built was indicated in historical documents (Medina, 1908), the confluence of the Carcarañá and Coronda rivers, in Santa Fe Province, Argentina (see Fig. 1a), there were no more details about its location that were left.

In 2006, an archaeological project began for locating and recovering evidence related to the Fort. A wide area of 17.5 ha at the mouth of the river Carcarañá was surveyed, collecting archaeological material from the surface and a number of boreholes, in order to analyze its distribution and identify a probable location for the Fort. A relatively-large number of European objects of the 16th century and artefacts from local manufacturers were found in a sector located in the village of Puerto Gaboto (Fig. 1a) (Cocco et al., 2011; Letieri et al., 2010), so we focused our investigations there.

According to the historical background (Medina, 1908), the Sancti Spiritus Fort and the surrounding buildings had been constructed with wood and tampered earth, usually known as tapia in this region. As no evidences were observed on the surface, it was expected that

* Corresponding author.
E-mail address: osella@df.uba.ar (A. Osella).

0926-9851/$ – see front matter © 2012 Elsevier B.V. All rights reserved.
doi:10.1016/j.jappgeo.2012.04.005

Fig. 1. a) Map of the site, in Puerto Gaboto village, Santa Fe, Argentina. b) Scheme of the area prospected with geophysical methods. Sectors A and B were covered with EMI and GPR. Solid lines indicate the positions of geoelectric dipole–dipole profiles.

only remains of the walls could exist in the subsoil, probably, with large amounts of damage.

Within this context, we decided to carry out a first geophysical prospecting to look for the structures of the Fort, and eventually determine the extent of the settlement. In this first stage, we applied GPR, EMI and electrical profiling, over an area of $35 \times 30\ m^2$. These complementary methods have proved to be successful for mapping different archaeological features, including mud walls (see e.g., Arciniega-Ceballos et al., 2009; Bongiovanni et al., 2008; Böniger and Tronicke, 2010; De Domenico et al., 2006; Francese et al., 2009; Martino et al., 2005; Osella et al., 2005). We designed these surveys to obtain the main characteristics of the near-surface region and compare the effectiveness of each method to detect the target structures. From different views of the acquired data, a number of signals probably originated by the historical Fort could be identified. These results were later confirmed through test excavations.

Once the presence of the Fort was established, the next aim was to obtain a detailed map of the structures, determine their continuity through the site with precision and resolve some areas that remained unclear from the first geophysical exploration. For this, during a second stage of geophysical investigations, we acquired high density grids of GPR data at a number of selected areas. Very-detailed maps were obtained, which were used to design a complete plan of excavations. These excavations allowed recognizing the remains of walls and also recovering an important amount of historical objects from the Fort as well as from previous and later settlements.

2. Methodology of the first geophysical surveys

The area under investigation did not present surface evidences of walls or bases of the Fort that could be used to obtain patterns of their electromagnetic responses and subsequently identify similar structures by comparison. Moreover, as the walls were constructed with material possibly extracted from the surrounding soil, low contrasts were expected between the physical properties of these structures and those of the embedding material. Therefore, we decided to use three complementary methods based on different physical properties, in order to improve the chances of detecting the targets. This also enabled to compare the effectiveness of each method for this application and to determine which of them was the most adequate for possibly performing high-density surveys to study the structures in detail.

The investigated area had dimensions 35 m × 30 m and almost-flat topography (Fig. 1b). We divided this area into two sectors: Sector A extended along the interval x = [0;17] m and Sector B along the interval x = [0;35] m. These sectors were prospected with GPR and EMI. Also, nine dipole–dipole geoelectrical profiles in the y-direction and two in the x-direction were acquired.

We conducted the GPR survey with a constant-offset methodology (Daniels, 2004). This allows to prospect large areas in minimal times, which is useful in initial stages of exploration. We used a Sensors & Software Pulse EKKO PRO radar unit, with 500 MHz antennas. This frequency often provides a good resolution and penetration for archaeological targets such as walls and other architectural structures. The sectors were covered with grids of parallel lines deployed along the x and y directions, respectively, with cross-line spacing 0.5 m and in-line sampling interval 0.025 m, which assured enough sampling density in both directions for this kind of targets. The stacking of traces was 16. To process and visualize the data we used software developed by our research group on Matlab platform. In addition, we also used the Reflex vs. 5.5.1 (2010), for comparison. The general processing flow for the data was the following: time zero correction, dewow filtering, background subtraction, broadband pass filtering in space and time, and application of gain. The dewow process was used to remove slow-decaying low-frequency signals that are induced due to the proximity of the transmitter, receiver and soil. If not removed, these signals tend to saturate sectors in the images of the data. The background subtraction was used to remove horizontal bands in the images, in particular, the direct waves, by replacing each trace by the original trace minus the average trace, calculated along all the traces in this case. The bandpass filtering was applied to remove frequency components outside the intervals of interest. The data were analyzed by representing them in standard vertical sections and constant-time slices of the amplitudes and intensities of the data. In the last case, the absolute value of the amplitude was averaged in time through a one-period interval before representing it. A mean propagation velocity was obtained by fitting hyperbolae to the diffraction hyperbolae in the vertical sections. This velocity was occasionally used to convert times to apparent depths.

For the EMI survey, we employed a multifrequency electromagnetic induction equipment Geophex GEM-2 (Won et al., 1996). This instrument basically consists of a transmitter and a receiver, which are two fixed and coplanar small coils, separated by a constant distance. The transmitter generates a controlled primary magnetic field at different frequencies, and the receiver detects the secondary magnetic field produced by the currents induced in the subsoil, which is decomposed into in-phase (*IP*) and quadrature (*Q*) components and expressed in ppm (parts per million) of the primary field. These components provide information about the electrical resistivity and magnetic permeability of the subsoil. The GEM-2 equipment has a frequency range from 330 to 47,970 Hz. As the depths of the targets were expected to be less

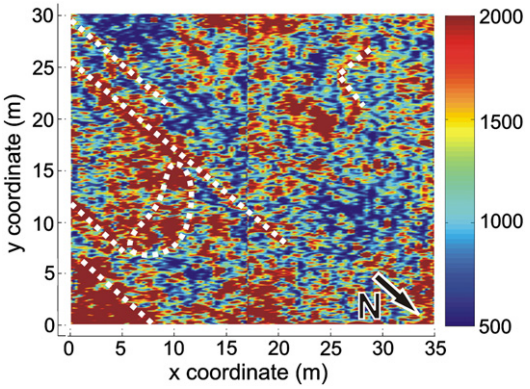

Fig. 2. Constant-time slice of the intensity of the GPR data acquired along the y-axis for t = 12 ns. The main detected features are indicated with dotted lines.

than 1–2 m, we selected relatively-high frequencies for the prospecting: 3925, 8775, 13,575, 20,175, 30,375 and 47,025 Hz. In both sectors data were collected in the orthogonal directions x and y, with line spacing 0.5 m. The transmitter–receiver azimuth was coincident with the direction of the survey lines (in-line surveys) and the axes of the dipoles were perpendicular to the ground (horizontal coils). Then, we performed the usual plan-view maps of the *IP* and *Q* components corresponding to each frequency.

The geoelectrical surveys (Reynolds, 1997) were performed with a multielectrode resistivimeter Scintrex Saris 500, employing the dipole–dipole configuration with electrode separation a = 0.75 m and maximum n = 6. We used this configuration because it generally provides better lateral resolution for shallow studies than the other common arrays (Locke, 2011). Nine 30 m long profiles, spaced 3 m between them, were acquired along the y-direction, from x = 0 m to x = 24 m (Fig. 1b). Two 35 m long profiles were acquired in the x-direction, at the positions y = 12 m and y = 14 m, respectively. To obtain 2D electrical images of the soil, we applied the RES2DINV inversion method (Loke and Barker, 1996). Then, the results corresponding to the profiles along the y-direction were transversally interpolated to generate a pseudo 3D model of the area.

3. Results of the first geophysical surveys

3.1. GPR results

Fig. 2 shows a constant-time slice of the intensity of the processed GPR data, for the y-oriented profiles and t = 12 ns, which correspond to an apparent depth of 0.65 m (mean velocity, v = (11 +/− 1) cm/ns). We saturated the color scales to make visible a number of areas that presented slightly higher intensities than the environment and distinctive geometries. Most of these areas were located in Sector A and had elongated aspects, with approximately-parallel borders along the north–south direction that formed an angle of about 45° with respect to the x and y axes (the straight lines in the figure indicate the centers of the areas). These characteristics suggested a probable cultural origin of the reflectors that produce them. Another area that was located between the previous and contained a group of relatively high intensity reflections also caught our interest; it has been delimited by a curved line in the figure. Finally, an anomaly with L form seemed to appear in Sector B. In general, these reflections extended in time from 5 ns down to 20 ns, depending on the sector, which implies a maximum apparent depth of 1.1 m.

Fig. 3 is an example of a vertical section of the GPR data. This figure corresponds to the profile located at x = 4 m, which crossed the elongated anomalies of Sector A. The positions of these anomalies have been indicated in the figure. Although this kind of graphs revealed some characteristics of the subsoil, only unclear interpretations of the detected anomalies could be obtained from them, mainly because the reflections in the radargrams presented rather complex and variable forms in the interval of interest (t≈[5–20] ns). Regarding this, structures as the ones expected here often have uneven borders due to partial collapses, which produce irregular reflections that are difficult to interpret (Bonomo et al., 2010). Furthermore, if the materials of the structures and the surroundings are similar, moderate to low intensity reflections result. Mixing of materials due to erosion further reduces the contrasts and thus the reflected amplitudes. In these cases, secondary reflections from surrounding objects can superimpose to the primary reflections and mask them.

3.2. EMI results

The EMI data corresponding to Sector A did not provide reliable or useful information because, at all frequencies, they were highly contaminated with electromagnetic noise generated by a nearby power line. This prevented the detection of anomalies associated to the Fort, which were not expected to be intense due to the probable low conductivity contrasts. On the other hand, the plan-views of the *IP* and *Q* components of Sector B detected the presence of a zone with low responses, which had two nearly linear and parallel borders, with the same direction as the main linear anomalies observed with GPR. As an example, Fig. 4 shows this anomalous zone on a graph of the *Q* component corresponding to the lines acquired in the y-direction, for one of the highest frequencies. Its borders are indicated with solid lines. The location of the lower border is almost coincident with the main linear anomaly observed in this sector with GPR (dashed line).

3.3. Dipole–dipole results

Fig. 5 shows constant-depth slices of the electrical resistivity of the area x = [0.24] m, y = [0.30] m, together with the main anomalies obtained with GPR (dashed lines) and EMI (solid lines) for comparison. Even though the spacing between these lines was relatively large (3 m), the cross-interpolation enabled tracking the anomalies. In particular, various linear features corresponding to transitional zones between areas with different resistivities were observed. The

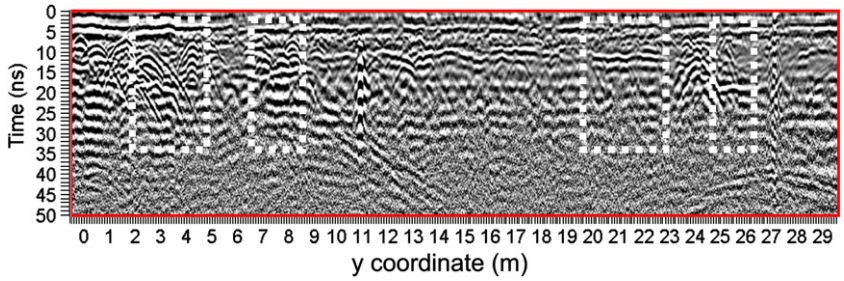

Fig. 3. Radargram obtained at x = 4.0 m. The positions of the linear features detected in the time slices, probably associated to anthropogenic structures, are marked with dotted lines.

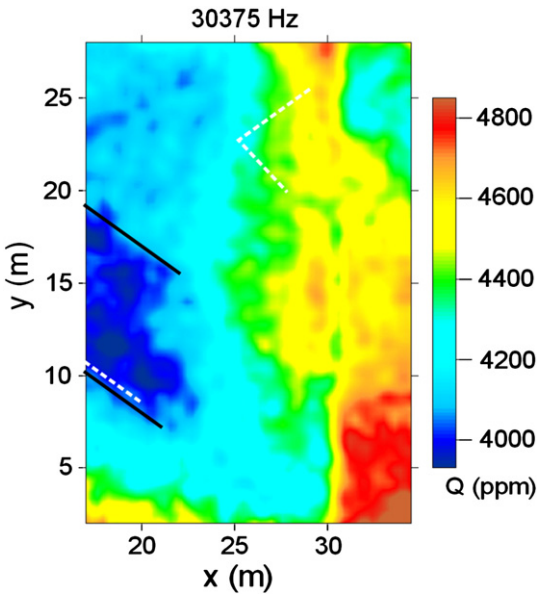

Fig. 4. Plan-views of the quadrature component in Sector B, at a representative frequency 30,375 Hz. Solid and dotted lines, respectively indicate the EMI and GPR anomalies detected in this sector.

main orientation of these features coincided with the ones obtained by the other methods.

In general, the distribution of anomalies obtained with the three geophysical methods, but especially with GPR, revealed the probable existence of linear anthropological structures that could be related to the Fort. To improve the quality of the maps, more-detailed surveying was needed at different areas of the two sectors. But previously, some excavations were carried out following the geophysical maps, in order to confirm the predicted features and their anthropological origin, and to evaluate the sensitivity of the three applied methodologies for detecting them.

4. Results of the first excavations

Fig. 6a is a map of the anomalous areas and associated features detected from the first geophysical works (marked with letters A–M). The shadowed zones indicate the excavated areas. The first stratum found was colluvial sediment mainly composed of silt and small portions of sand. Below 25 cm deep, we began to observe horizontal changes in the characteristics of the sediment, at both sides of features A, B, C and D. Going deeper, the differences in the sediment became more evident. At 40–45 cm deep, three parallel anthropogenic structures were identified, which occupied the areas between the features (Fig. 6b): 1) a ditch between D and C, 2) a tapia wall between C and B and, 3) a smaller ditch between B and A.

The analysis of the structures and the sediment around them allowed knowing that during their construction, a consolidated-silt natural layer was firstly removed from the soil in the area of the structures. Then, the tapia wall was built up just on the boundary of the regional Tezanos Pinto Formation (TPF, Iriondo and Paira, 2007), using TPF loess probably extracted from the larger ditch, which extended slightly inside this formation. This kind of aeolian sediment was probably used because it has greater plasticity and capacity of compaction than the shallowest sediment and the intermediate silt. This material was put inside a wooden formwork build up at the wall position and compressed by tampering. At the moment of the excavation, the tapia presented clear signs of erosion and partial collapses throughout the years. Sediments had filled the large ditch, where we found archaeological material of local and European manufactures from the 16th century. At the bottom of the ditch, there was a 20 cm thick layer of sediment that contained charcoal and remains of entire glass beads (tubular, circular), slabs of fused beads, glazed pottery, majolica, native potsherds, bone dices, iron studs and burned woods.

A burial of a native settler was found inside the shallow sediment, which produced the anomalous reflections in the area of feature E. We estimated that this burial corresponded to a period after the Fort destruction in 1529. On the other hand, differences between the sediment at both sides of feature F were observed from approximately 25 cm deep, as occurred with features A and D. At 35 cm deep, the aforementioned consolidated-silt stratum was found, again with a discontinuity at both sides of the feature. Considering the very-similar characteristics of features A, D and F, we estimated that F also had a probable anthropological origin.

In general, identifying the features detected by the geophysical surveys was difficult in both excavated areas, mainly because the archaeological structures and the soil around them presented quite-akin aspects due to their compositions and the mixing of materials produced by partial collapses of the structures. Tracking these structures through both areas was also complicated since they presented irregular shapes. Therefore, at this point, we interrupted the excavations to perform additional geophysical surveys to obtain more detailed information at different sectors.

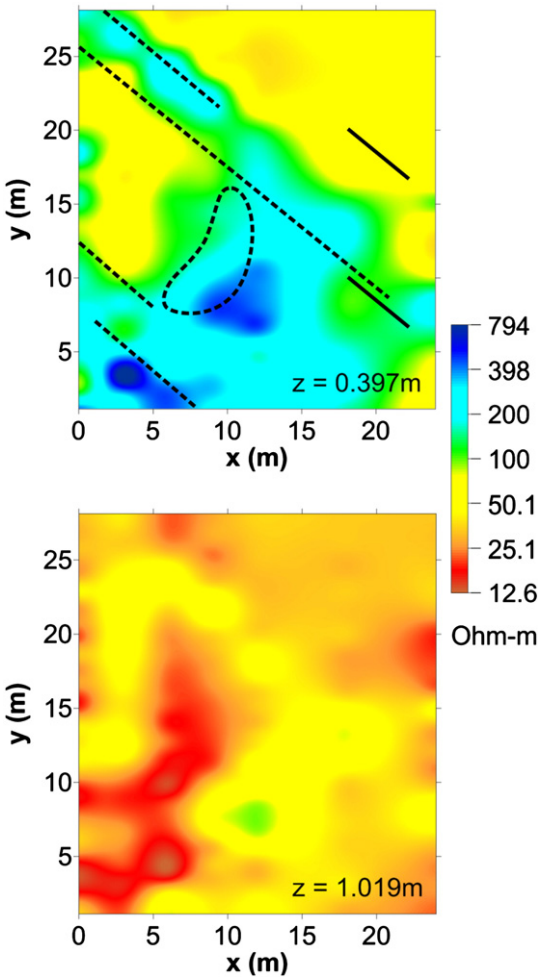

Fig. 5. Constant-depth slices of the electrical resistivity model obtained from the dipole–dipole geoelectic data. The main anomalies detected with GPR (dotted lines) and EMI (solid lines) are drawn for comparison.

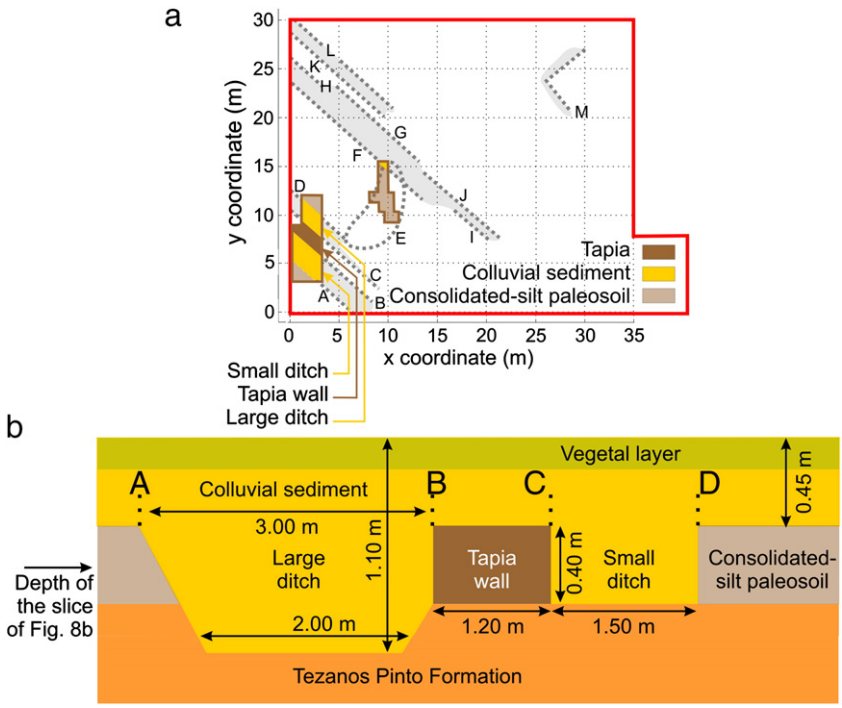

Fig. 6. a) Map of the main anomalous areas and features detected in the first geophysical surveys (named with letters A–M). The areas of the first excavations and the structures found in them are also shown. b) Vertical schema of the structures found in the area of features A, B, C and D.

4.1. Methodology of the second geophysical surveys

The results of the excavations performed at specific positions confirmed the reliability of the applied geophysical methodologies for detecting the archaeological structures. In particular, the GPR methodology was more sensitive to these structures than the EMI and electrical methodologies, and provided the most detailed maps of them. For this reason, we decided to continue our investigations only with GPR.

In this stage of investigations, we acquired high-density grids of constant-offset GPR profiles (Grasmueck et al., 2005). We prospected some sub-areas of Sectors A and B, to better define the continuity of the detected structures, to characterize them in more detail and to investigate a number of confusing reflections possibly related to other linear features. A problem we faced during the initial investigation was that the reflections at the archaeological structures tended to be hidden in some sectors by the reflections at the tree roots. For example, in the sector of the south-eastern excavation, the reflections at the roots were numerous and had similar or higher intensities than the reflections at the structures. Furthermore, the roots presented nearly-rectilinear segments, which produced reflections that were occasionally misinterpreted as produced by the borders of architectural structures, mainly due to insufficient cross resolution. Then, acquiring high-density grids of data could aid to distinguish both kinds of reflectors, in particular, by allowing tracking them through constant-time slices. Finally, migrating 3D data volumes could further improve the resolution, making possible a simpler and more precise interpretation.

Fig. 7 shows the sub-areas prospected during the second GPR surveys, which were named S1, S2, S3 and S4. These areas were selected with the main goals of studying the detected features in more detail and determining their continuity through the site. Additionally, in the area S4, some reflections with unclear linear characteristics had been observed during the first surveys. Then, another objective in S4 was to further investigate these anomalies. All the areas were covered along the y-direction, with 5 cm cross-line spacing and 0.025 cm sampling interval. The stacking of traces was 16.

5. Results of the second geophysical surveys

5.1. Sector S1

In general, the analysis of the data of this sector enabled tracking features A, B, C and D with precision, as well as different roots that could be easily distinguished from the archaeological structures. We could determine that features A, B, C and D extended toward the North beyond the positions predicted by the first prospecting, reaching the borders of S1. Fig. 8a shows the trajectories of these features on a constant-time slice of the migrated data (t = 18 ns). To obtain this figure, we applied 3D f–k migration with a migration velocity equal to the mean propagation velocity, (8.4 +/− 0.6) cm, measured in this second prospection. This procedure was also used in the

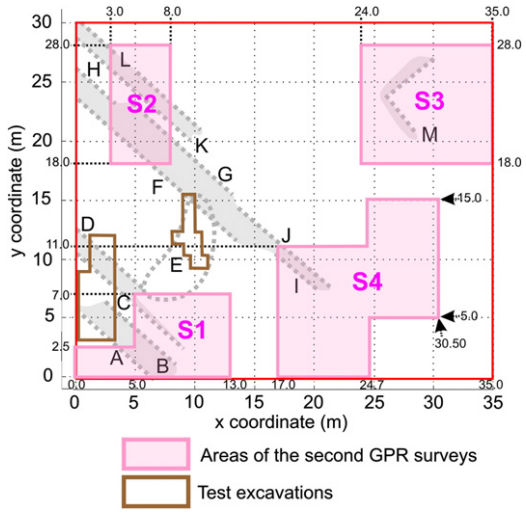

Fig. 7. Plan of the sectors covered with high density GPR prospecting during the second geophysical works.

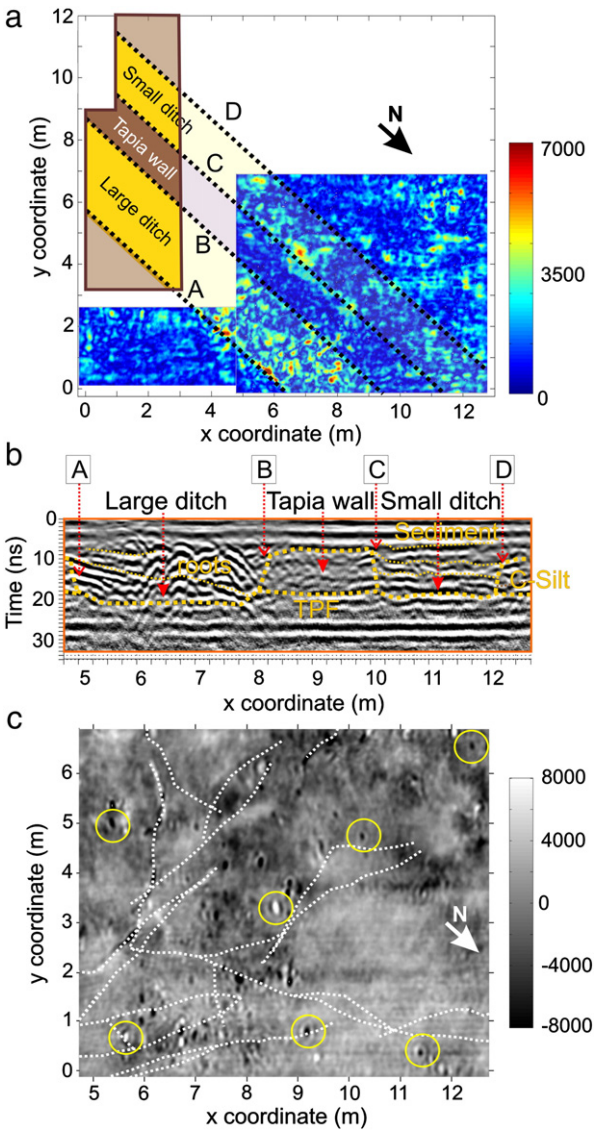

Fig. 8. a) Constant-time slice of Sector S1, for profiles acquired along the y direction and t = 18 ns. The data have been migrated and their intensity averaged in one-period intervals. The dotted lines indicate the positions of features A, B C and D and their correlation with the results of the previous test excavations, b) vertical section of the data acquired along the x direction, for y = 1 m, and its interpretation, c) constant-time slice of the data, for t = 5.5 ns. Solid lines indicate the positions of small approximately-circular reflectors, and dotted lines the trajectories of different tree roots.

migrated sections of the next paragraphs. The area of the large ditch presented the highest density of reflectors, including roots and different sediment layers, from time 5 ns to 20 ns, as can be observed in the vertical section of Fig. 8b. The last time corresponded to the bottom of the ditch, at an approximate depth of 110 cm. These reflections produced the overall high-intensity response observed between features A and B in Fig. 8a and during the first prospecting (Fig. 2).

Reflections at the sides and bottom of the small ditch produced the intermediate-intensity area located between features C and D, which had uneven forms in the horizontal and vertical (temporal) directions (Fig. 8b). Finally, the relatively low-intensity area located between features A and B was a consequence of weak reflections at the top and bottom boundaries of the wall, along most of the wall segments, and by almost-negligible reflections from the inside, due to the homogeneity of the wall materials. The low contrast at the top interface of the wall was probably related to moderate differences between both media and significant deterioration of the structure (as observed during the first excavations), whereas at the bottom interface, to very-similar media.

Several reflections at approximately-circular objects, with diameters 20–40 cm, were observed through the entire sector, below 3–4 ns. Some of them have been indicated in Fig. 8c (solid lines), which is a constant-time slice of the data for t = 5.5 ns. In this figure, we have also indicated reflections at the tree roots (dotted lines). In relation to the circular reflections, their characteristics resembled those of reflections at cylindrical objects, which seemed to go through the consolidated-silt layer interface. This information was relevant since, as the Fort had been constructed with tapia and wood, these reflections could correspond to marks of wooden poles.

5.2. Sector S2

In this sector, we observed a lower number of roots than in S1 but a greater number of circular reflectors (possible marks of poles), which began to appear between 5 ns and 7 ns. In particular, a group of them was found approximately aligned with feature G (Fig. 9a) and seemed to form a linear structure.

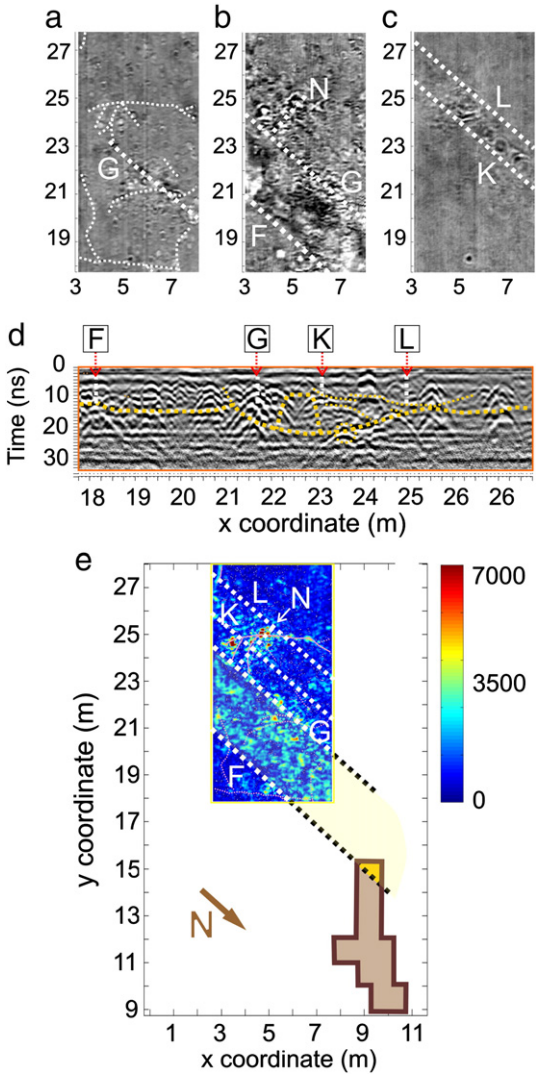

Fig. 9. Constant-time slices of Sector S2 for a) t = 7.0 ns, b) 15.0 ns and c) 23.0 ns. The lines indicate the main features in each of them. d) Vertical section of the data, for x = 6.0 m, and its interpretation. e) Constant-time slice of the migrated data, for t = 15.0 ns. The main features detected in S2 are summarized and their correlation with the results of the nearest test excavation is shown.

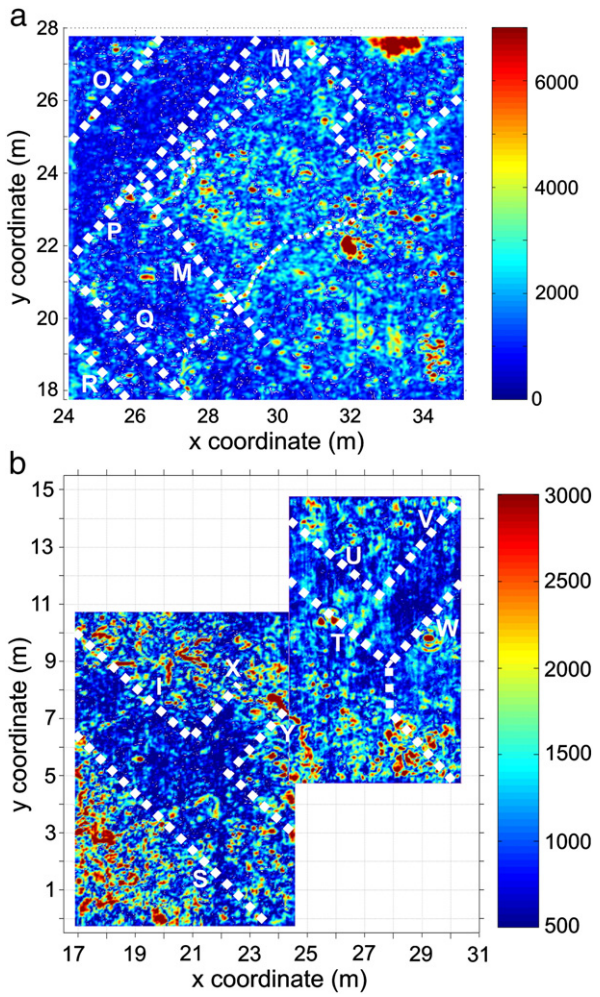

Fig. 10. a) Constant-time slices of the migrated data of S3, for t = 8.2 ns. The polygonal corresponds to feature M, which bounded a plateau. Other features detected in the sector have been indicated with letters O–T. b) Constant-time slice of Sector S4, for t = 13.4 ns. The lines indicate the main features found there.

A reflection at a rather-smooth interface appeared between features F and G, at t = 13–15 ns (Fig. 9b). This reflection produced the main anomaly detected in the sector during the first prospecting. We also found that feature G extended toward the south further than originally predicted and that a second transversal feature composed of approximately-aligned circular reflections appeared between features G and K (feature N in Fig. 9b).

A third group of approximately-circular reflectors was located along the center of the area bounded by features K and L, at times 17–20 ns (Fig. 9c). As the other two groups in S2, we interpreted them as probable footprints of wooden posts forming structures related to walls or their construction. Above these circular reflectors and up to approximately 10 ns, reflections at a number of sediment layers appeared (Fig. 9d). They produced the other relatively-high intensity zone detected during the first survey. Finally, a rather-homogeneous zone appeared between features G and K, at times 9–20 ns, which had characteristics that resembled the response of the tapia wall in S1. Fig. 9e summarizes the main results for Sector S2.

5.3. Sector S3

Several approximately-circular reflectors, similar to those observed in Sectors S1 and S2 were found in S3 between 3 ns and 8 ns, although they were not aligned as the groups in S2. Below them, a reflection from a smooth interface was observed. This reflection occurred at 12–15 ns, at the borders of S3, and rose to 6–9 ns toward the center of S3, where it exhibited a plateau. Feature M coincided with the large borders of the plateau (Fig. 10a), which presented a geometrical form that suggested an anthropogenic origin. We also detected two elongated areas with relatively-low intensities, which extended in depth almost from the surface to the smooth interface (areas O–P and Q–R in Fig. 10a, respectively).

5.4. Sector S4

In the shallowest parts of S4, we observed many circular reflectors, as those described in the previous sections, at times below 3–5 ns. From these times, different features could be observed, which delineated a number of low-intensity areas, possibly related to mud walls (Fig. 10b). Although feature J did not appear in the images of S4, we observed that feature I coincided with one of the detected features, continuing toward the northern boundary of the area, beyond the position predicted during the first prospecting.

6. Results of the second excavations

After the high-density GPR surveys, the excavated area was extended to a total of 150 m^2, (Fig. 11a). During the excavation, the linear and small circular features predicted by the geophysical methods in this area were corroborated (Fig. 11b). These features were related to different kinds of construction techniques associated to the settlement of the Sancti Spiritus Fort and village as well as previous and

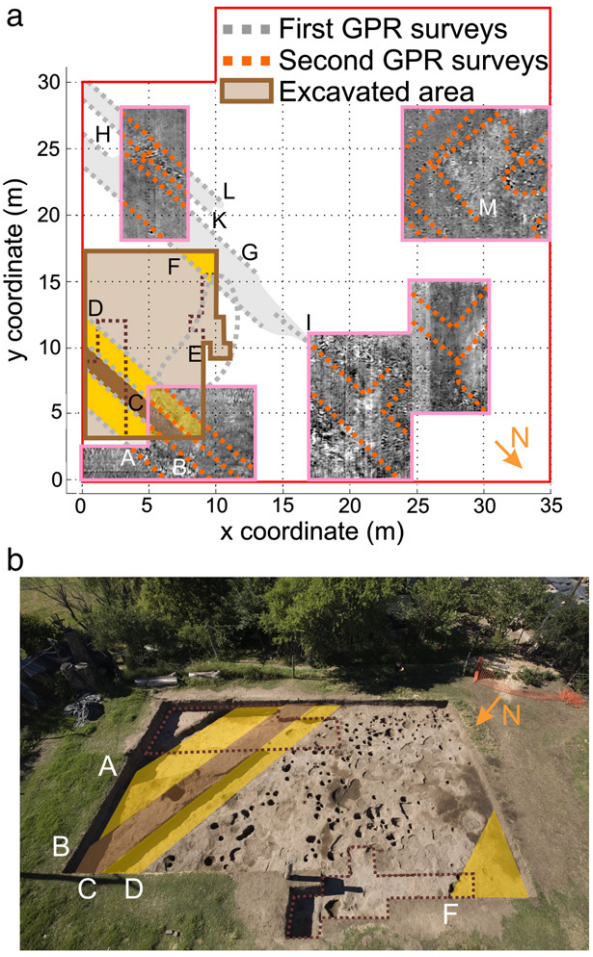

Fig. 11. a) Final map of the main features and the excavated areas, superimposed to constant-time slices of the second GPR surveys. Confirmed structures have been shadowed in the figure, as in Fig. 7b, b) overall picture of the second stage of excavations.

later aboriginal settlements. Regarding the Sancti Spiritus Fort, we confirmed that the large ditch and the tapia wall integrated its structure. When the Fort and the village were burned down, the wall began to deteriorate. Today only its base remains, together with the ditch from which most of the archaeological artefacts were recovered. The circular holes corresponded to prints of poles that were used by the natives in their constructions before the Spaniards. They were located in the consolidated-silt layer that was later cut by the Spaniards during the construction of the Fort. Finally, the presence of aboriginal artefacts and skeletal remains of fauna inside the holes and ditches indicated the posterior reuse of the site by the natives.

7. Conclusions

The GPR, EMI and geoelectric methodologies initially applied to localize the Fort, were sensitive to the structures in spite of their low electromagnetic contrasts, including the case of a tapia wall. The GPR method was the most sensitive for the detection and provided the best resolved maps of the structures. In a second stage of the geophysical investigations, an increment in the density of the GPR profiles made possible to study in great detail a number of sub-areas, analyzing the continuity of the detected structures and also a number of reflections that had remained unclear from the first study. The resulting images enabled tracking these structures with precision, as well as detecting new linear features and several small holes of poles. Also, the reflections at many tree roots could be identified and easily distinguished from the primary reflections at the archaeological structures. This significantly simplified the interpretation. A final map of the archaeological structures was obtained, from which extensive excavations were planned, optimizing the archaeological fieldwork.

From the geophysical perspective, this work presented two interesting challenges. On the one hand, to find the Fort from which there was no surface evidence, and on the other, to characterize its remains, which had low contrast with respect to the embedding material and were in poor conditions of conservation. Both difficulties were satisfactorily overcome through the applied methodology, and a detailed characterization of the soil was obtained.

From the archaeological point of view, the results were significant. In addition to finding this first Spanish settlement in the South Cone of America, abundant Spanish and Aboriginal materials were recovered, and also evidences of previous and later occupations, including a burial site, were found. This provided relevant data about the population dynamics of the site. It is important to point out that the excavations showed that the Fort remains were so damaged that without the aid of the maps obtained from the geophysical surveys, identifying and tracking them probably would not have been possible. The geophysical images, especially the high-density GPR maps, allowed overcoming these difficulties and guided the excavations in areas particularly difficult because of collapses, thus preventing further damage to the structures.

Acknowledgments

This work was supported by CONICET (Consejo Nacional de Investigaciones Científicas y Técnicas) and CFI (Consejo Federal de Inversiones).

References

Arciniega-Ceballos, A., Hernandez-Quintero, E., Cabral-Cano, E., Morett-Alatorre, L., Diaz-Molina, O., Soler-Arechalde, A., Chavez-Segura, R., 2009. Shallow geophysical survey at the archaeological site of San Miguel Tocuila, Basin of Mexico. Journal of Archaeological Science 36, 1199–1205.

Astiz, M.E., 1998. Impacto cultural de un enclave europeo del siglo XVI: Sancti Spíritus. Book: Homenaje a Alberto Rex Gonzalez. 50 años de aportes al desarrollo y consolidación de la antropología Argentina. Publisher: Facultad de Filosofía y Letras, UBA, Buenos Aires, Argentina, pp. 177–180.

Astiz, M.E., Tomé, A., 1987. Localización y Descripción de Sancti Spiritus. Journal: Cuadernos, No. 12. Publisher: Instituto Nacional de Antropología, Buenos Aires, Argentina, pp. 203–251.

Bongiovanni, V., Bonomo, N., de la Vega, M., Martino, L., Osella, A., 2008. Rapid evaluation of multifrequency EMI data to characterize buried structures at a historical Jesuit Mission in Argentina. Journal of Applied Geophysics 64, 37–46.

Böniger, U., Tronicke, J., 2010. Integrated data analysis at an archaeological site: a case study using 3D GPR, magnetic, and high-resolution topographic data. Geophysics 75 (4), B169–B176.

Bonomo, N., Osella, A., Ratto, N., 2010. Detecting and mapping a buried building with GPR at an ancient village in Northwestern Argentina. Journal of Archaeological Science 37, 3247–3255.

Carbia, R.D., 1914. Book: Historia eclesiástica del Río de la Plata, vol. I, pp. 1536–1673. Publisher: Alfa y Omega. Buenos Aires, Argentina

Cocco, G., Letieri, F., Frittegotto, G., 2011. El descubrimiento y estudio del Fuerte Sancti Spíritus. Journal: Revista América. Publisher: Centro de Estudios Hispanoamericanos, Santa Fe, Argentina, pp. 69–85.

Daniels, D., 2004. Ground Penetrating Radar. In: Daniels, David J. (Ed.), The Institution of Engineering and Technology, London, pp. 1–723.

De Domenico, D., Giannino, F., Leucci, G., Bottari, C., 2006. Integrated geophysical surveys at the archaeological site of Tindari (Sicily, Italy). Journal of Archaeological Science 33, 961–970.

Francese, R., Finzi, E., Morelli, G., 2009. 3-D high-resolution multi-channel radar investigation of a Roman village in Northern Italy. Journal of Applied Geophysics 67, 44–51.

Grasmueck, M., Weger, R., Horstmeyer, H., 2005. Full-resolution 3D GPR imaging. Geophysics 70, K12–K19.

Iriondo, M., Paira, A., 2007. Physical geography of the basin. In: Iriondo, Paggi, Parma (Eds.), The Middle Parana River, Limnology of a Subtropical River. Springer Verlag, Berlin, pp. 7–32.

Letieri, F., Cocco, G., Frittegotto, G., Astiz, M.A., 2010. Investigaciones arqueológicas sobre el primer asentamiento español en la cuenca del Río de la Plata: el fuerte Sancti Spíritus (1527–1529). In: Chiavazza, H., Ceruti, C.N. (Eds.), Arqueología de ciudades americanas del Siglo XVI. Publisher: Facultad de Filosofía y Letras, UNCuyo, Mendoza, Argentina, pp. 275–315.

Locke, M.H., 2011. Tutorial: 2D & 3D electrical imaging surveys. Geotomo Software Malaysia. http://www.geoelectrical.com/, http://www.geotomosoft.com/.

Loke, M.H., Barker, R.D., 1996. Rapid least-squares inversion of apparent resistivity pseudosections by a quasi-Newton method. Geophysical Prospecting 44, 131–152.

Martino, L., Bonomo, N., Lascano, E., Osella, A., Ratto, N., 2005. Electrical and GPR joint prospecting at the Palo Blanco archaelogical site, NW Argentina. A case history. Geophysics 71 (6), 193–199.

Medina, J. T. 1908. Book: El veneciano Sebastián Caboto. Al servicio de España y especialmente de su proyectado viaje a Las Molucas por el estrecho de Magallanes y al reconocimiento de la Costa del Continente hasta la Gobernación de Pedrarias Dávila. Vol. I and II., 1247 pp. Publisher: Imprenta y Encuadernación Universitaria. Santiago de Chile, Chile

Osella, A., de la Vega, M., Lascano, E., 2005. 3D electrical imaging of an archaeological site using electric and electromagnetic methods. Geophysics 70 (4), 101–107.

Outes, F., 1902. El primer asentamiento Español en territorio Argentino. Noticia histórico-geográfica, Buenos Aires, pp. 1527–1529.

Reflex vs. 5.5.1, 2010. Software for 2D Processing and 2D/3D Interpretation of GPR Data. Sandmeier Scientific Software, Germany.

Reynolds, J., 1997. An Introduction to Applied and Environmental Geophysics. John Willey & Sons, West Sussex, pp. 1–778.

Won, I.J., Kreiswetter, D.A., Fields, G.R.A., Sutton, L., 1996. GEM-2: a new multifrequency electromagnetic sensor. Journal of Environmental and Engineering Geophysics 1 (2), 129–137.

Zapata Gollan, A., 1979. La primera urbanización hispanoamericana en el Río de la Plata: Santa Fe. Journal: Boletín del Centro de Investigaciones Históricas y Estéticas, No. 24. Publisher: Universidad Central de Venezuela: Facultad de Arquitectura y Urbanismo, Caracas, Venezuela, pp. 50–59.